Article

Monitoring long-term cardiac activity with contactless radio frequency signals

Bin-Bin Zhang [1,2], Dongheng Zhang[1], Yadong Li [3], Zhi Lu [1], Jinbo Chen [1], Haoyu Wang [1], Fang Zhou[1], Yu Pu[1], Yang Hu[1], Li-Kun Ma [2], Qibin Sun[1,4] & Yan Chen [1,2] ✉

Cardiovascular diseases claim over 10 million lives annually, highlighting the critical need for long-term monitoring and early detection of cardiac abnormalities. Existing techniques like electrocardiograms (ECG) and Holter are accurate but suffer from discomfort caused by body-attached electrodes. While wearable devices using photoplethysmography offer more convenience, they sacrifice accuracy and are susceptible to environmental interference. Here we present a radio frequency (RF)-based (60 to 64 GHz) sensing system that monitors long-term heart rate variability (HRV) with clinical-grade accuracy. Our system successfully overcomes the orders-larger interference from respiration motion in far-field conditions without any model training. By identifying previously undiscovered frequency ranges (beyond 10-order heartbeat harmonics) where heartbeat information predominates over other motions, we generate prominent heartbeat patterns with harmonics typically considered detrimental. Extensive evaluations, including a large-scale outpatient setting involving 6,222 eligible participants and a long-term daily life scenario, where sleep data was collected over 5 separate random nights over two months and a continuous 21-night period, demonstrate that our system can monitor HRV and identify abnormalities with comparable performance to clinical-grade ECG-based systems. This RF-based HRV sensing system has the potential to support active self-assessment and revolutionize medical prevention with long-term and precise health monitoring.

According to the World Health Organization (WHO), cardiovascular diseases (CVDs) account for approximately 17.9 million deaths annually and result in an estimated cost of around $555 billion per year[1,2]. This makes CVDs the leading cause of global mortality and a significant burden on national healthcare systems[3,4]. The crucial step towards preventing CVDs is early detection, as over 80% of premature CVD cases, occurring before the age of 75, can be prevented through prompt diagnosis and timely treatment[5,6].

Long-term and continuous monitoring of cardiac activities plays a pivotal role in the early detection of CVDs, considering that initial-phase symptoms may not be pronounced or easily identifiable[7,8]. Consequently, without extended monitoring that spans weeks or even months, it is highly possible to overlook abnormalities. However, existing detection techniques face challenges in achieving long-term and precise monitoring of cardiac activity. Specifically, clinical devices such as electrocardiogram (ECG)[9] and Holter[10] record the heart's

[1]School of Cyber Science and Technology, University of Science and Technology of China, Hefei, China. [2]The First Affiliated Hospital of USTC, Division of Life Science and Medicine, University of Science and Technology of China, Hefei, China. [3]Department of Electrical and Computer Engineering, University of Washington, Seattle, WA, USA. [4]Zhongke Radio Sensing AI Technology Co., Ltd, Hefei, China. ✉e-mail: eecyan@ustc.edu.cn

electrical signals, which healthcare professionals analyze to identify cardiovascular conditions[11]. Despite offering medical-grade accuracy, they require multiple body-attached electrodes, leading to uncomfortable user experiences and thus not suitable for long-term usage. While other wearable devices[12–14] might be more convenient and portable, most of them are based on photoplethysmography (PPG)[15], which is less accurate and susceptible to external influence such as ambient light and skin condition[16,17]. Consequently, individuals often postpone examinations until they experience discomfort or symptoms related to their heart or overall health. This delay in seeking diagnosis and treatment can further exacerbate the condition.

Recent studies have demonstrated the potential of wireless signals in the mobile health-sensing field[18–20]. Leveraging the fact that radio frequency (RF) signals are non-contact, privacy-preserved, and reflect subtle mechanical vibrations caused by heartbeat, RF-based systems have been widely studied for the long-term monitoring of various cardiac activity indicators, including heart sound[21], seismocardiogram[22,23], and HRV[24–26]. Among them, HRV, the variation in time intervals between successive heartbeats, has been validated as an effective prognostic indicator for CVDs[27–30]. To extract HRV from RF signals, which is a superimposition of respiration and heartbeat motions, existing methods[24,25] employ frequency domain techniques to separate reflections into different frequency bands based on respiration rate and heartbeat rate. However, the major challenge is that the magnitudes of the respiration motion (at the centimeter scale) are orders larger than that of the heartbeat motion (at the sub-millimeter scale). As a result, there is substantial spectral leakage of the respiration motion into the heart rate frequency band, leading to a low signal-to-interference-plus-noise ratio (SINR) for the heartbeat signal (see more information in Supplementary Note 2 and Fig. 1). In such a case, the estimation of HRV performance is generally poor. To address the issue, existing work by Sharma et al.[31] leverages a near-field radio-frequency (RF) sensor worn at the thorax to reduce the influence of abdomen motion caused by respiration. However, respiration can still lead to a certain level of thorax motion, which is significantly larger than heartbeat motion. Zhang et al.[32] propose to learn the mapping between RF signal and heartbeat waveform with deep neural networks. Nevertheless, their black-box machine learning model requires massive training data to generalize across different individuals.

Here, we report an RF-based sensing system (i.e., RF-HRV) that achieves long-term HRV monitoring with clinical-grade accuracy. RF-HRV successfully overcomes the orders-larger interference from respiration motion in far-field conditions without any model training. Our system overturns conventional signal processing frameworks that only extract the fundamental frequency of heartbeat signals within the heart rate frequency band. Specifically, we propose to leverage previously undiscovered higher frequency ranges (beyond 10-order heartbeat harmonics) where heartbeat information dominates over other motions. The key insight is that the harmonics of respiration motions decay more rapidly than those of heartbeats. This is because the lower frequency of respiration compared to heartbeats results in higher-order respiratory harmonics that decay at a faster rate. Nevertheless, extracting heartbeat signals from frequencies far from the heart rate frequency band presents unique challenges, including the rapid attenuation of signal strength and the unknown order of heartbeat harmonics. Fortunately, we discovered another important phenomenon, namely the beat frequency effect, which means that when two harmonics are superimposed, they generate a distinctive signal pattern with a frequency equal to the difference between the frequencies of the two harmonics. Therefore, by superimposing adjacent heartbeat harmonics, we can produce specific heartbeat patterns that exhibit a frequency precisely equal to the heart rate. Such an approach marks a significant difference from

traditional views that harmonics are detrimental and should be suppressed.

To comprehensively evaluate RF-HRV, we conduct extensive experiments in a large-scale outpatient setting involving 6222 participants with various cardiac conditions, and a long-term daily scenario including 5 separate random nights over two months and 21 consecutive nights for the same subject. Our system demonstrates a median real-time inter-beat interval (IBI) error of 26.1 ms and 34.1 ms in the outpatient and daily scenarios, respectively, representing about tenfold improvement compared to existing systems that extract signals solely from the heart rate frequency band. Furthermore, we explore the potential of RF-HRV for automated classification of heartbeat abnormalities, showing that our contactless system achieves comparable performance with clinical-grade ECG-based systems that require 12 body-attached electrodes. By shifting the focus from post-disease treatment to proactive prevention, our system shows immense potential in providing a comprehensive understanding of an individual's health conditions in their own homes, thus paving the way for a new era of personalized and remote healthcare integrated into the daily lives of millions of people.

Results

We conducted a comprehensive evaluation of our system on three specific tasks illustrated in Fig. 1e. Firstly, we monitored HRV in a large-scale outpatient setting involving 6,222 participants. Secondly, we leveraged the estimated HRV to identify different heart abnormalities with those outpatient data. Lastly, we assessed the capability of our system in a long-term daily life scenario, where sleep data was collected with 5 separate random nights over two months and a continuous 21-night period to demonstrate its practicability.

The RF device utilized in our study is depicted in Fig. 1b. It comprises a radar module TI AWR6843aop responsible for transmitting and receiving millimeter-wave signals (see more details in Supplementary Table 9 and Fig. 8), along with a communication module for transmitting the collected data to a laptop for subsequent signal processing. During the data collection process, as illustrated in Fig. 1d, participants lay on a bed, while the radar sensor was positioned approximately 60 centimeters above them, facing downwards towards the chest. In the outpatient scenario, each recorded RF signal lasted for 30 seconds, and in the long-term daily life scenario, data is collected for 5 to 7 hours each night.

To quantitatively assess the performance of our system, we employed real-time inter-beat interval (RT-IBI) as an important metric to evaluate the real-time performance of our system, which can reflect the real-time capture capability of the monitoring method for heartbeat changes (see more details in Supplementary Note 6 and Figures 5–6). Additionally, we also employed another three widely recognized HRV metrics[33]: root-mean-squared of the successive IBIs differences (RMSSD), the standard deviation of all the IBIs (SDRR), and the percentage of successive IBIs that differ by more than 50 ms (pNN50). Among these metrics, RMSSD and pNN50 measure short-term changes in heart rate while SDRR is a global indicator reflecting the long-term variation in heart rate. All of them stand for the health status of the heart. Detailed definitions of these four metrics can be found in the Method section. The ground-truth data was obtained through ECG measurements using body-attached electrodes[34]. We compared our system with two recent RF-based HRV monitoring methods, namely mmHRV[24] and V2iFi[25]. Our reported results of V2iFi and mmHRV are obtained by re-implementing these algorithms and running them on our dataset. Moreover, we compared our algorithm with a deep learning algorithm, and the results indicate that the learning-based method has comparable yet slightly inferior performance compared to our method (see more details in Supplementary Note 11 and Fig. 11).
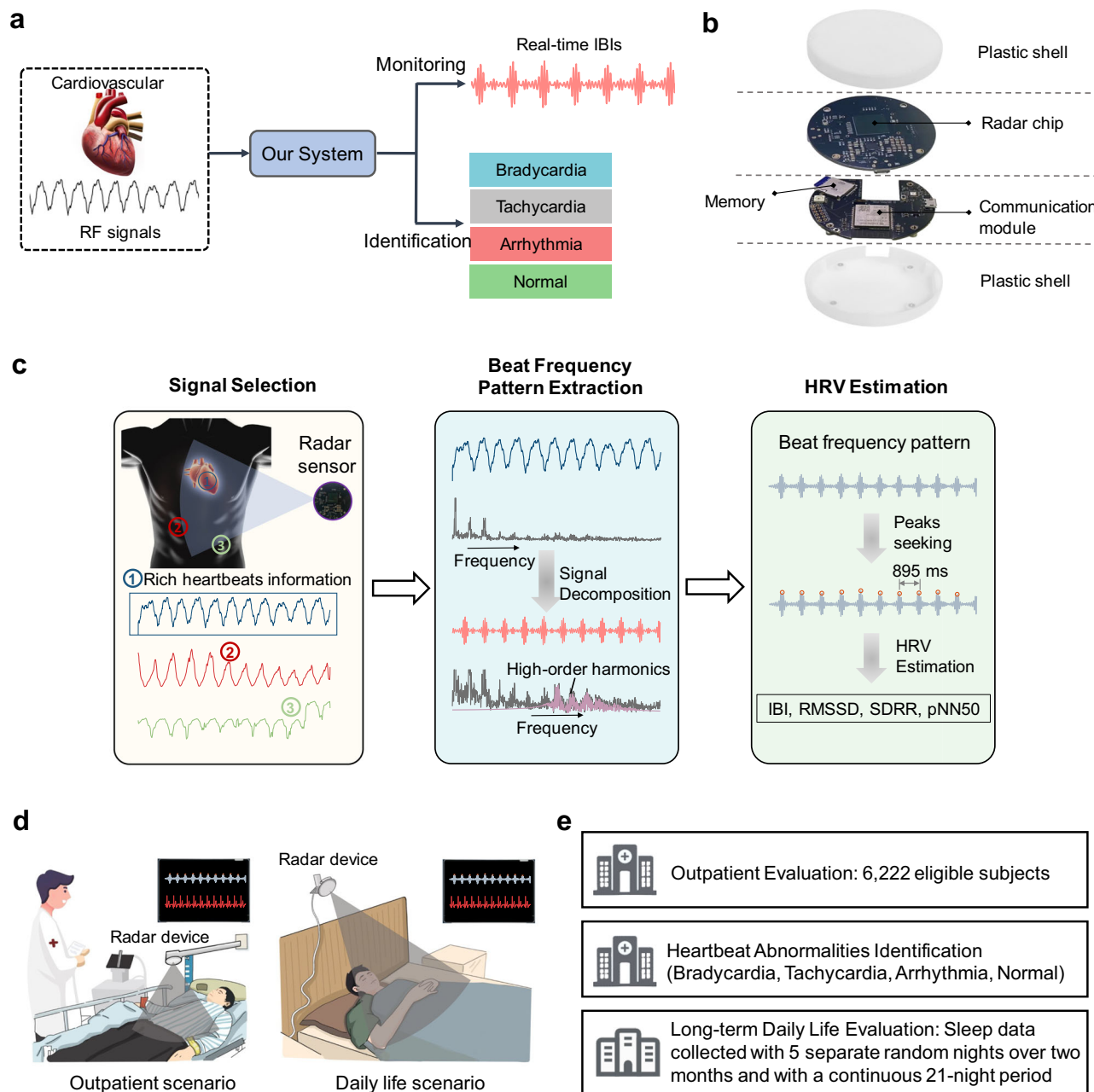
Fig. 1 | Overview of the proposed system. a Our system takes the RF signals reflected from the chest as input and outputs the real-time inter-beat interval (RT-IBI), which is then utilized to identify heart disease. **b** Schematic exploded-view of the RF device used in this paper. **c** Our system consists of three components: signal selection, beat frequency pattern extraction, and heart rate variability (HRV) estimation. Firstly, we introduce a signal selection algorithm to select a voxel point with abundant heartbeat information. Then, we decompose the signal into various frequency components and use high-frequency components to obtain the beat frequency pattern. Lastly, we extract heartbeat peaks from the pattern to calculate HRV. **d** The proposed system is evaluated under two scenarios: the outpatient scenario and the daily life scenario. **e** The proposed system is evaluated on three tasks, including monitoring HRV in large-scale outpatient settings, heartbeat abnormalities identification, and monitoring HRV in long-term daily life scenario.

Large-scale outpatient evaluation

We first assessed the performance of our system with a large-scale outpatient dataset collected from a top-tier tertiary hospital. The dataset consists of 6,222 eligible participants with ages ranging from 3 to 94, and the detailed information of the participants' baseline characteristics is shown in Table 1.

Figure 2a–d depict the performance of our system against two baseline methods with the four metrics mentioned above. Specifically, our system achieved a median RT-IBI error of 26.1 ms, a median RMSSD error of 53.8 ms, a median SDRR error of 33.7 ms, and

a median pNN50 error of 11.1%, all of which are significantly lower than baselines. It is noteworthy that compared with mmHRV and V2iFi, which have a median RMSSD error of 632.3 ms and 569.1 ms, respectively, our system achieved over 10x improvement in estimating the variations of successive IBI. This is because the heart rate variability information within the heart rate frequency band is overwhelmed by respiratory leakage, rendering existing methods unable to accurately monitor HRV within this frequency range. In contrast, our system accurately captures the variability of heart rate intervals by extracting heartbeat information in the high-

Table 1 | Baseline demographic and characteristics

	Dataset 7090 subjects (eligible 6222)
Excluded from analysis	
Loosening of the electrode pads	868
Eligible subjects	6222
Age (Years)	55 ± 16 (3-94)
Gender	
Male	2817 (45.3%)
Female	3405 (54.7%)
ECG and laboratory findings	
Sinus rhythm	5423 (87.2%)
Sinus bradycardia	428 (6.9%)
Sinus tachycardia	137 (2.2%)
Arrhythmia	245 (3.9%)
Left BBB	21 (0.3%)
Right BBB	125 (2.0%)
ST-segment changes	872 (14.0%)
T-wave changes	434 (7.0%)

Values are mean + -s.d. (minimum-maximum) or *n* (%).
Simultaneous occurrences of different categories are present in ECG and laboratory findings.

frequency band, where heartbeat information dominates over other motions.

To better illustrate the performance distribution of our method across the entire large-scale dataset, we present the comparison of the cumulative distribution function (CDF) of the four metrics for these three methods in Fig. 2e–h. Compared to existing methods, our method achieves significantly lower HRV estimation errors in the majority of the participants. Furthermore, in Fig. 1i, we present three qualitative examples of HRV estimation under different cardiac conditions, showcasing the precise RT-IBI estimating capabilities of our system.

Heartbeat abnormalities identification
Given that HRV serves as a crucial indicator of cardiac conditions, our system can be effectively employed for diagnosing common CVDs. In this context, we utilize a simple rule to classify cardiac conditions into four categories: normal, bradycardia, tachycardia, and arrhythmia. This classification is based solely on the mean and variance of IBIs. Specifically, if individuals' average IBI exceeds 1000 ms, they are identified with bradycardia. Conversely, if their average IBI falls below 600 ms, they are classified as having tachycardia. For individuals with an average IBI between 600 ms and 1000 ms, their classification as normal or arrhythmia is determined by the variance of the IBI. If the variance is below a certain threshold, they are considered to be in a normal condition. However, if the variance exceeds the threshold, they are identified with arrhythmia.

To evaluate the diagnostic performance of our system on a large-scale outpatient dataset, we analyzed the proportions and age distribution of the four cardiac conditions, as depicted in Fig. 3a. The ground truth of the cardiac conditions was determined by cardiologists who analyzed the participants' ECGs.

In Fig. 3b, we present a performance comparison for diagnosing heart diseases with the estimated IBI using different methods. The confusion matrix reveals that our system achieved an average classification accuracy of 83.4%, demonstrating a significant improvement over mmHRV's 65.3% and V2iFi's 69.6%. Specifically, our system achieved diagnosis accuracies of 85.9%, 92.2%, and 93.9% for normal, bradycardia, and tachycardia, respectively.

We also noticed that the diagnosis accuracy for arrhythmia was only 47.6%. However, we believe that this low accuracy for arrhythmia can primarily be attributed to the simplicity of the features used in our classification approach, which may not be robust enough to provide accurate results for this specific condition. To support this argument, we present the classification performance using IBIs obtained from ground truth ECG data in Fig. 3c. Interestingly, we can observe that even when using ECG data, the accuracy for diagnosing arrhythmia is still only 53.9%. Additionally, we investigated the impact of the variance threshold on the diagnostic accuracy of RF-HRV, as depicted in Fig. 3d. We increased the variance threshold from 50 to 120 while keeping other settings unchanged. The results in Fig. 3d show that the system achieves the best performance with a threshold of 90. However, as the threshold changes, the system's performance deteriorates rapidly, indicating that relying solely on the mean and variance of the IBIs is inadequate for a robust classification. As a result, future studies can explore more advanced techniques, such as machine learning, to achieve improved classification performance for heart abnormalities.

Long-term daily life evaluation
In addition to outpatient evaluations, we also assess the long-term monitoring capabilities of our system in overnight sleep settings. Specifically, we collected RF signals from the same participant over 5 separate random nights, with a time spanning 2 months. During the monitoring process, the radar device was positioned one meter above the participant, with the antenna directed toward the torso. For RF data acquisition, we employed a TI AWR6843aop mmWave device, which operates within the frequency range of 60-64 GHz. To obtain the ground truth of HRV, we utilized a polysomnography (PSG) device to monitor ECG data and various physiological indicators.

To facilitate analysis, the overnight data was segmented into multiple slices of equal time intervals using a sliding window approach. The duration of each slice is 30 seconds when dividing the sleep data (The HRV computation time for different signal epochs is depicted in Supplementary Table 8). Slices containing significant body motion, as indicated by pronounced RF signal variations, were excluded from further analysis (Notice the drastic changes in the phase shown in Supplementary Fig. 9). The ratio of usable epochs in our long-term recordings is approximately 80.8%. Each remaining slice was then input into our system, which extracted IBIs as output. These extracted IBIs were subsequently compared to the ground truth to calculate the estimation error for HRV.

The comparative performance of our system against two baseline methods, as evaluated using the aforementioned four metrics, is presented in Fig. 4b–e. Specifically, RF-HRV achieved a median IBI error of 34.1 ms, a median RMSSD error of 62.2 ms, a median SDRR error of 38.8 ms, and a median pNN50 error of 10.7%. Compared to mmHRV and V2iFi, our system significantly outperformed them across all evaluation metrics and achieved over 10x improvement in estimating RMSSD and SDRR. To provide a clearer overview of how our system performs across the entire long-term dataset, we depict the comparison of CDF of the four metrics in Fig. 4f–i. It can be seen that our system consistently exhibits notably lower HRV estimation errors across the majority of participants when compared to existing systems. These results demonstrate that our system is capable of effectively monitoring HRV over an extended duration.

Furthermore, we observed a slight decline in the performance of HRV monitoring during this experiment, in comparison to outpatient evaluations. This discrepancy can be attributed to the specific conditions of long-term HRV monitoring during sleep. In this scenario, the radar device was angled towards the subject's chest, which led to a reduction in the SNR of the collected radar signals. Additionally, participants naturally assume different positions during sleep, and certain positions may impact the accuracy of HRV monitoring.
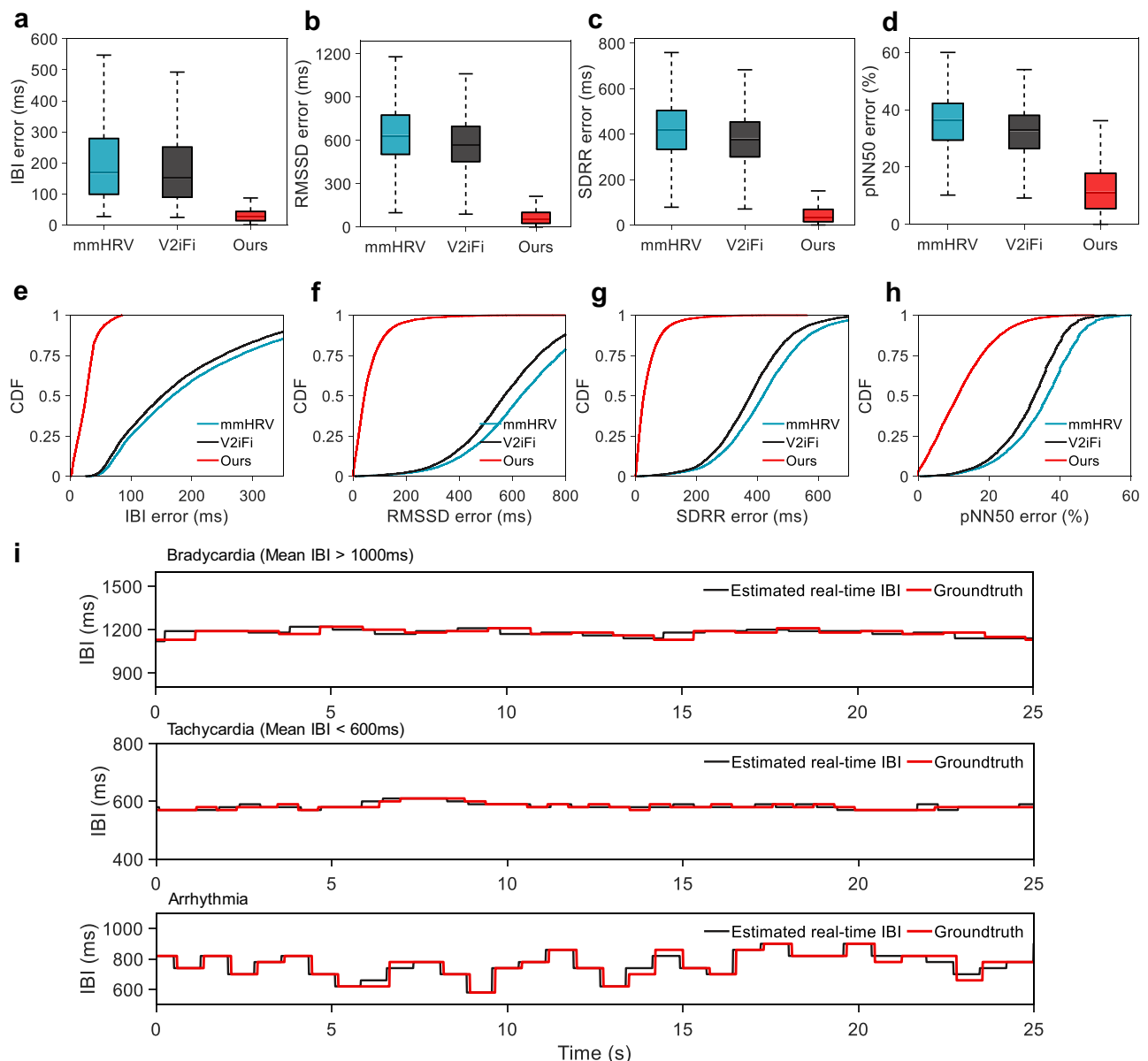
Fig. 2 | Evaluation in the large-scale outpatient setting. a Comparison of real-time inter-beat interval (RT-IBI) error. Our system achieves a 26.1 ms median RT-IBI error, while mmHRV and V2iFi achieve 168.3 ms and 151.6 ms median RT-IBI error, respectively. **b** Comparison of root mean square of the successive differences (RMSSD) error. RF-HRV achieves a 53.8 ms median RMSSD error, while mmHRV and V2iFi achieve 632.3 ms and 569.1 ms median RMSSD error, respectively. **c** Comparison of standard deviation of all normal R-R intervals (SDRR) error. RF-HRV achieves a 33.7 ms median SDRR error, while mmHRV and V2iFi achieve 419.4 ms and 377.5 ms median SDRR error, respectively. **d** Comparison of proportion of N-N intervals exceeding 50 ms (pNN50) error. RF-HRV achieves 11.1% pNN50 error, while mmHRV and V2iFi achieve 36.4% and 32.8% median pNN50 error, respectively. **e–h** The cumulative distribution function (CDF) plots of RT-IBI error, RMSSD error, SDRR error, pNN50 error. **i** The RT-IBI estimated by our system from three heartbeat abnormalities. $n = 6,222$ outpatient data points in box plots of **a**–**h**. Square, mean; minima, smallest non-outlier value; maxima, largest non-outlier value; center line, median; box bounds, upper and lower quartiles; whiskers, 1.5 × interquartile range, in box plots of **a**–**d**.

Additionally, to further assess the system's capability for long-term and continuous monitoring, we have supplemented an experiment with 21 consecutive nights of monitoring. The experimental results are consistent with the aforementioned results from the 5 random nights of monitoring (For more details, see Supplementary Note 10 and Fig. 10).

Ablation study

In this section, we investigated the impact of different modules and various parameters of RF-HRV on its performance. Specifically, we introduced a signal selection algorithm designed to identify the signal with the most informative heartbeat information among multiple voxels' reflected signals. To demonstrate the effectiveness of this algorithm, we compared it with three existing signal selection algorithms: mmHRV[24], Mtrack[35], and BNR[36]. Results indicate that our proposed algorithm outperforms the others in terms of RT-IBI error, with values of 26.1 ms for our algorithm, 36.6 ms for mmHRV, 45.2 ms for Mtrack, and 40.1 ms for BNR, as shown in Fig. 5a. We also calculated the accuracy of selecting the signal with the richest heartbeat information. As illustrated in Fig. 5b, our algorithm achieved an accuracy of 79.3%, surpassing the performances of mmHRV (62.1%), Mtrack (58.7%), and BNR (60.4%) (see Fig. 5b). These results demonstrate the superiority of our proposed signal selection algorithm.
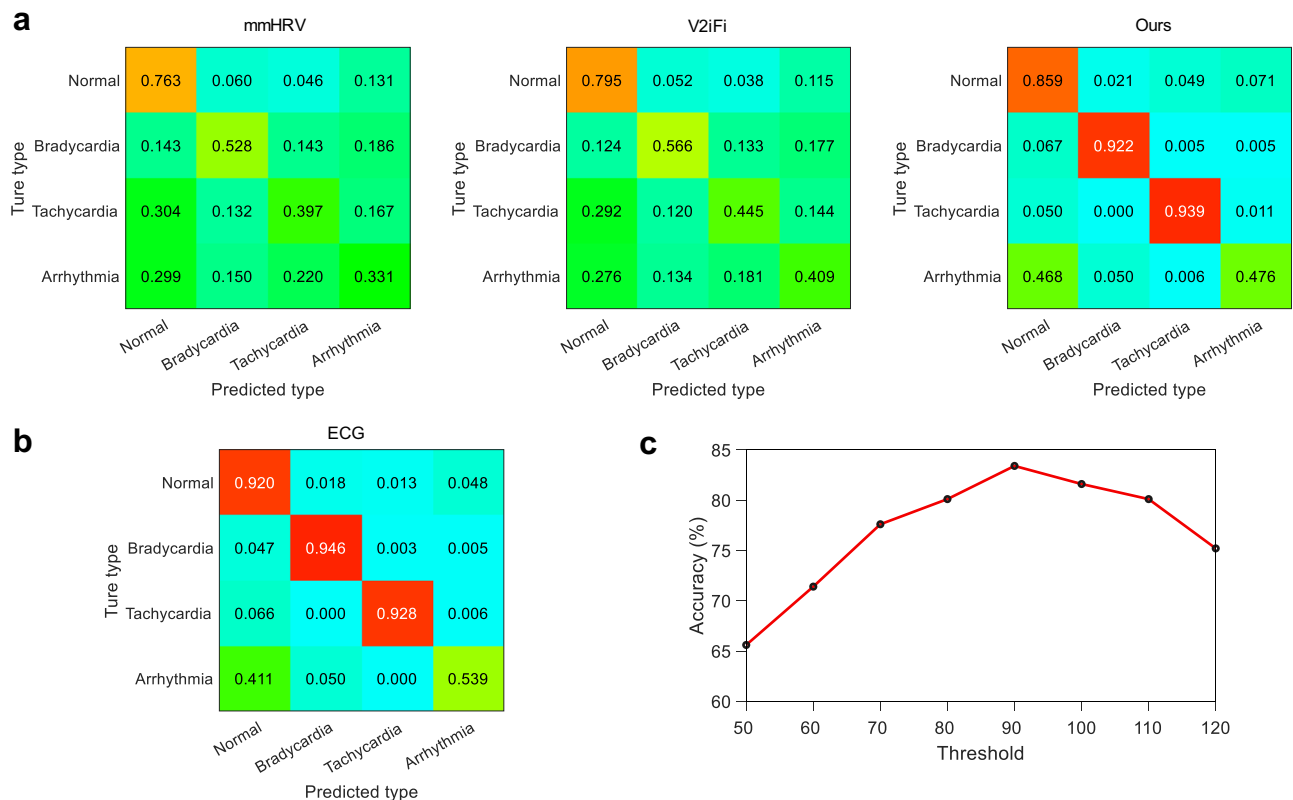
Fig. 3 | Evaluation of heart abnormalities identification. a The performance comparison in diagnosing heartbeat abnormalities between RF-HRV and existing methods. RF-HRV achieved an average classification accuracy of 83.4%, marking a substantial improvement compared to mmHRV's 65.3% and V2iFi's 69.6%. Our system performs well in identifying bradycardia and tachycardia, while only has an accuracy of 47.6% in arrhythmia due to the simplified features and classification algorithm. **b** The overall identification accuracy of the ECG device is 90.6%, while only has an accuracy of 53.9% in arrhythmia. **c** The classification results of our system when using different thresholds.

In the beat frequency pattern extraction step, we employ the variational mode decomposition (VMD) algorithm to extract the high-frequency component from the raw RF signal. This allows us to obtain clean and accurate heartbeat patterns in comparison to existing methods that extract heartbeat patterns within the heart rate frequency band. Figure 5d illustrates the decomposition of the raw RF signal into five components, namely Imf 1 to Imf 5 (Intrinsic Mode Functions). These components cover a frequency range from low to high, as depicted in Fig. 5e. Imf 5 corresponds to the high-frequency component containing the heartbeat patterns. On the other hand, Imf 3 represents the component within the heart rate frequency band, and utilizing this component to estimate heartbeat patterns would yield poor results due to respiratory spectra leakage and interference.

Furthermore, we conducted a comparison between the VMD algorithm, which we utilized to obtain the heartbeat patterns, and two other methods: band-pass filtering (BPF)[37] and second-order difference (SOD)[38]. The results, as shown in Fig. 5c, indicate that the VMD algorithm outperformed the other two methods, which can be attributed to the VMD's ability to extract the high-frequency component that contains a richer set of heartbeat information.

Moreover, we have compared the performance of our method with that of PPG devices. The results indicate that our method achieved better performance on RT-IBI, but in the other three aspects (RMSSD, SDRR, pNN50), PPG demonstrated better performance. In summary, our method achieves, in a completely non-contact manner, comparable performance with PPG (see more details in Supplementary Note 7).

We have also conducted additional experiments to investigate the impact of several critical factors on system performance, including variations in sensor angle, different distances to the user, multiple layers of clothing, and the postures of the subjects (For more details, see Supplementary Note 8).

Discussion

Here we presented a long-term and precise HRV monitoring system with RF signals, which has the potential to achieve long-term monitoring of heart conditions that spans weeks or even months. Past solutions fall short of long-term monitoring, which is crucial for the early detection of diseases. Specifically, traditional methods like ECG or wearable devices cause additional burdens or provide less accuracy. Consequently, individuals tend to seek medical intervention only when they experience evident symptoms, missing the opportunity to detect and control the disease development at an early stage. In contrast, our RF-based system offers a non-intrusive and precise approach to HRV monitoring and eliminates any burdens or inconveniences for individuals. This enables continuous monitoring over extended periods without direct contact with the body. By employing our system, individuals can proactively identify HRV anomalies as early as possible through long-term monitoring, which allows for timely intervention and medical treatment.

While the existing radar-based cardiac monitoring[39–41] is gaining increasing attention in both academia and industry, a fundamental challenge, namely the substantial spectral leakage of the respiration motion into the heart rate frequency band, remains unresolved. Some studies[42,43] reduce the interference of respiratory harmonics by utilizing the second or third harmonics of heartbeats, but none of them have theoretically analyzed how respiratory harmonics might affect heartbeats. In contrast, we have found that due to the amplitude of respiration being much greater than that of heartbeats, even the fourth, fifth, or higher-order respiratory harmonics have energy similar
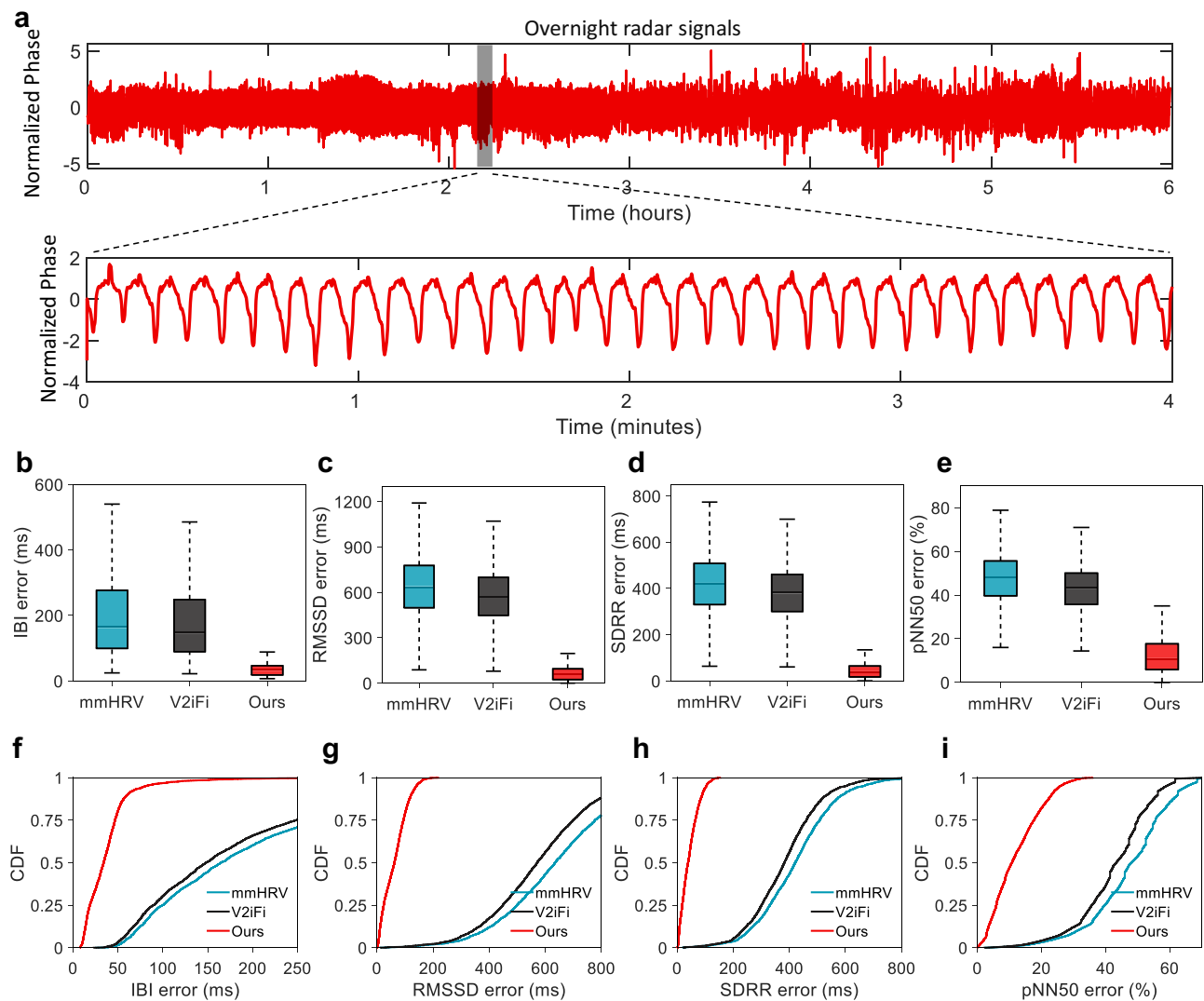
Fig. 4 | Evaluation in long-term daily life scenario. a Overnight radar signals. The radar signals throughout the night were collected when the subject was sleeping. **b** Comparison of real-time inter-beat interval (RT-IBI) error. RF-HRV achieves a 34.1 ms median RT-IBI error, while mmHRV and V2iFi achieve 164.6 ms and 147.9 ms median RT-IBI error, respectively. **c** Comparison of root mean square of the successive differences (RMSSD) error. RF-HRV achieves a 62.2 ms median RMSSD error, while mmHRV and V2iFi achieve 635.3 ms and 571.2 ms median RMSSD error, respectively. **d** Comparison of standard deviation of all normal R-R intervals (SDRR) error. RF-HRV achieves a 38.8 ms median SDRR error, while mmHRV and V2iFi

achieve 421.1 ms and 382.3 ms median SDRR error, respectively. **e** Comparison of proportion of N-N intervals exceed 50 ms (pNN50) error. RF-HRV achieves a 10.7% pNN50 error, while mmHRV and V2iFi achieve 48.1% and 43.3% median pNN50 error, respectively. **f**–**i** The cumulative distribution function (CDF) plots of RT-IBI error, RMSSD error, SDRR error, and pNN50 error. $n = 5$ nights data in box plots of (b-i). Square, mean; minima, smallest non-outlier value; maxima, largest non-outlier value; center line, median; box bounds, upper and lower quartiles; whiskers, 1.5 × interquartile range, in box plots of (b-e).

to the fundamental frequency of the heartbeat. Consequently, these higher-order respiratory harmonics can still intermingle with the fundamental frequency or second/third harmonics of heartbeats (For more details, see Supplementary Note 2 and Fig. 1), which leads to existing works cannot support long-term and accurate cardiac monitoring, especially for large-scale populations.

To address this issue, we systematically analyze the impact of higher-order harmonics and observe a simple and fundamental yet unidentified phenomenon: respiration harmonics decay more rapidly than heartbeat harmonics. Leveraging this discovery, we develop the core insight that differs from existing works[42–45], i.e., we extract more clean heartbeat information leveraging frequency ranges much higher than existing work, typically beyond 10-order heartbeat harmonics. Based on the insight, we successfully extract heartbeat signals from frequencies far from the heart rate frequency band leveraging the beat frequency effect. Specifically, we find that when two harmonics are

superimposed, they generate a distinctive signal pattern with a frequency equal to the difference between the frequencies of the two harmonics. Therefore, we generate strong heartbeat patterns that exhibit a frequency precisely equal to the heart rate by superimposing adjacent higher-order heartbeat harmonics.

In this work, we have validated the superior performance of our system in short-term monitoring (30s) across large-scale populations (6222), as well as long-term monitoring (multiple nights) for a single subject. For a more comprehensive evaluation of the outpatient study, long-term validation on a large-scale population is necessary but yet to be implemented, which requires excessive resources recruiting more participants with additional funding support. Moreover, we demonstrate the long-term monitoring capability of our system in single-person scenarios because our focus is to address the interference of respiratory leakage on heart rate estimation. However, in practice, two or more people may need to be monitored simultaneously. In such a
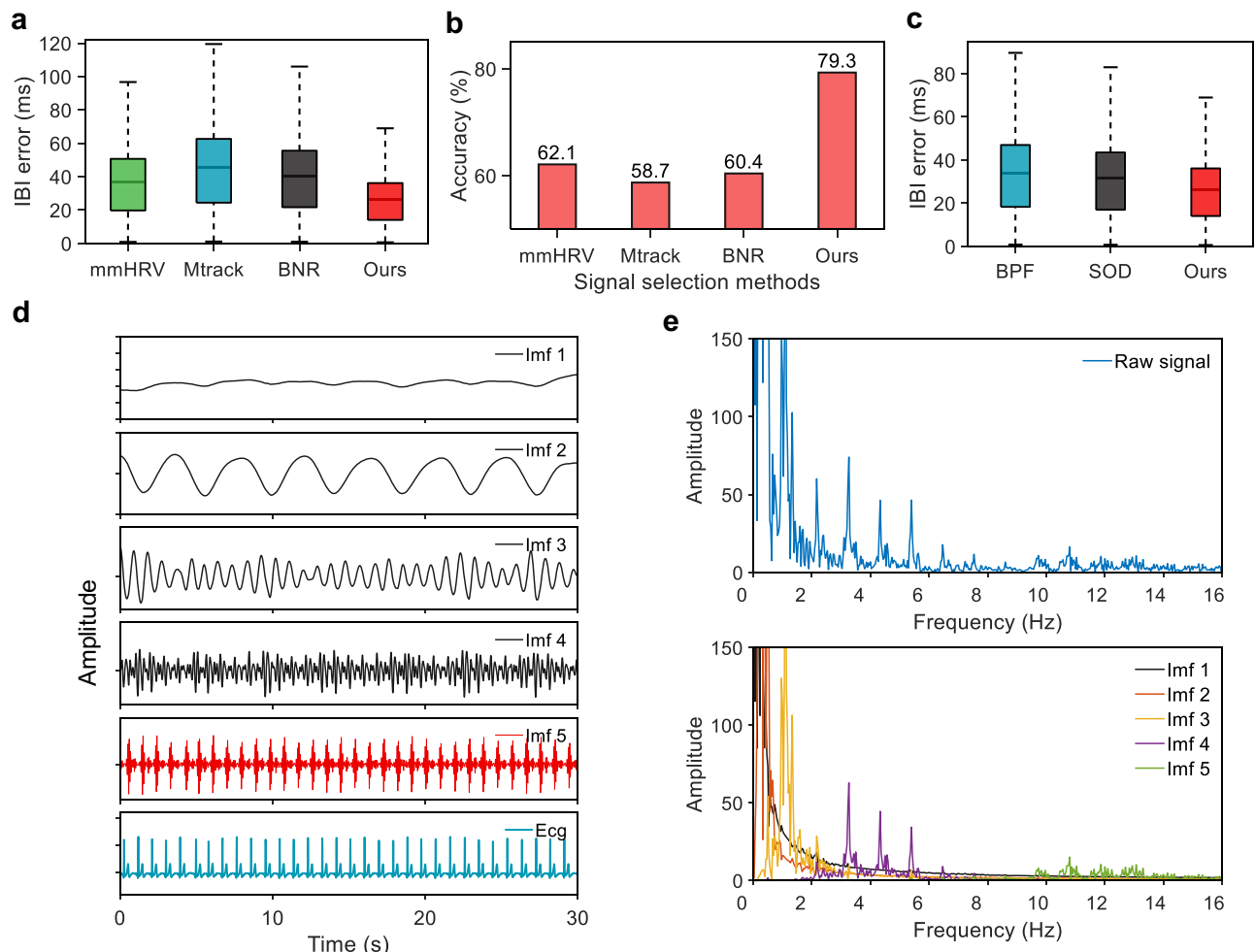
Fig. 5 | Ablation study. a We compared three signal selection algorithms (mmHRV[24], Mtrack[35], and BNR[36]) with our proposed algorithm while keeping other modules the same as RF-HRV. Our algorithm outperformed the others in terms of real-time inter-beat interval (RT-IBI) error (Ours: 26.1 ms, mmHRV: 36.6 ms, Mtrack: 45.2 ms, BNR: 40.1 ms). **b** We calculated the ratio of the selected optimal signal to all signals. Our signal selection algorithm achieved a ratio of 79.3%, surpassing mmHRV (62.1%), Mtrack (58.7%), and BNR (60.4%). **c** We compared the impact of several methods, including band-pass filtering (BPF) and second-order difference (SOD), for obtaining high-frequency components on the system performance. **d** Five different decomposed components. Imf 1 denotes the direct component of the signal, Imf 2 represents the respiratory signal, and Imf 5 is the high-frequency component, showing clear heartbeat information. **e** Frequency distribution of raw signal and different components. n = 6,222 outpatient data points in box plots of **a**–**c**. Square, mean; minima, smallest non-outlier value; maxima, largest non-outlier value; center line, median; box bounds, upper and lower quartiles; whiskers, 1.5 × interquartile range, in box plots of **a**, **c**.

case, the signals reflected by them may interfere with each other, requiring additional signal processing for multi-person sensing. Furthermore, most experiments in this work are predominantly in the scenario of an individual at rest in bed. This activity presents hours of a day for people, the investigation of heart activity monitoring during sleep is of significant importance for the early identification and prevention of underlying health conditions. Nevertheless, real-world applications often involve other short-term activities such as walking or exercising. Addressing these more dynamic scenarios, which are both significant and challenging, is crucial. We will dedicate more research efforts to advance the proposed HRV monitoring technique for covering a wider range of activities. While our primary focus has been on signal processing, we acknowledge the potential for hardware-level improvements to enhance SNR and signal quality. In future iterations, we plan to explore additional techniques, such as frequency division and advanced antenna designs, to further optimize system performance. Regarding motion artifact detection, sensor fusion would be a promising solution. In future work, we plan to explore the integration of other wireless signals, such as ultrasound, to improve accuracy under motion artifacts.

In summary, our system demonstrates how wireless signals can be leveraged to achieve long-term healthcare monitoring and early detection of medical abnormalities. By continuously monitoring individuals over an extended period without frequently visiting hospitals, such technology has the potential to pave the way for a new era of personalized and remote healthcare that can improve outcomes and prevent complications for millions of people.

Methods
Data preprocessing
In our RF-based HRV monitoring system, the raw signals obtained from the RF device consist of 2-dimensional channels (3 × 4) for each time frame. These channels correspond to the signals received by 3 transmitting antennas and 4 receiving antennas. To process these raw signals, we first apply the range Fast Fourier Transform (FFT) and angle FFT to each time frame of the signals. This transforms the signals into a 3-dimensional representation, specifically a range-angle-time representation. (see 2D FFT in Supplementary Note 1).

Once we have the range-angle-time representation, we employ the Constant False Alarm Rate (CFAR) algorithm[46] to detect the range

and angle bin of the subject of interest, which is crucial for further analysis and extraction of the heartbeat information from the RF signals.

System design

Signal selection. In our system (Fig. 1c), the received signals contain multiple reflections that cover the entire torso. However, not all parts of the torso contain a significant amount of heartbeat information. Hence, selecting the signal that contains rich heartbeat information is crucial for obtaining high SINR heartbeat patterns and achieving accurate HRV estimation[38].

Existing methods such as mmHRV[24], Mtrack[35], and BNR[36] have attempted to address this problem but have not fully met the requirements. In our paper, we introduce a signal selection algorithm to identify the signal with rich heartbeat information from multiple detected signals. This algorithm leverages the fact that for the same person, a signal with richer heartbeat information leads to a more stable estimation of IBI[47].

To implement the signal selection algorithm, we input the signals from multiple reflections into the system and separately obtain the IBIs for each signal. After applying the beat frequency pattern extraction, we obtain the heartbeat patterns and estimate the IBIs for each signal. Next, we calculate the variances of the estimated IBIs for each signal separately and choose the signal with the smallest variance in the estimated IBI as the optimal signal. This selection process ensures that the signal with the most reliable and consistent heartbeat information is chosen for further analysis and HRV estimation (see more details about signal selection in Supplementary Note 5).

Beat frequency pattern extraction. In contrast to existing methods[24,25], which focus on suppressing interference from respiratory motion within the heart rate frequency band, we propose a novel approach to extract the heartbeat information from a higher frequency band containing clean heartbeat information (see effects of heartbeat harmonics in Supplementary in Note 3 and Figure 2). Specifically, we employ a technique called VMD[48] (see Supplementary Note 5), which has been proven effective in decomposing the raw signal into several frequency components[49,50].

In our method, we specifically utilize the high-frequency component to extract the heartbeat information. Moreover, the high-order harmonics of the heartbeat present in the high-frequency component exhibit the beat frequency effect, resulting in highly complete and accurate heartbeat patterns (see the principle of beat frequency effect in Supplementary Note 4 and Fig. 3).

HRV estimation. After obtaining the heartbeat patterns, the next step is to detect the peaks within these patterns. One challenge in peak detection is the variation in amplitudes of the heartbeat patterns. To overcome this issue and improve the accuracy of peak detection, we propose a method that dynamically adjusts the threshold used in the peak-finding algorithm. Once the peaks are identified, we calculate the time interval between two successive peaks, which corresponds to the IBIs. Moreover, from the sequence of IBIs, we can calculate various HRV features, which can be leveraged to identify different cardiac abnormalities.

Implementations

In our implementation, the clinical ECGs were collected by the clinical-grade 12-lead ECG device. The daily life long-term 3-lead ECGs were obtained using Sid Medical HA301B Holter device. Code was written using Python version 3.9 (python software Foundation, PyTorch version 2.0.1) and Matlab R2021a. The hardware used for data processing and system execution is a Lenovo ThinkPad VE13GTSC laptop equipped with an Intel Core i7 processor and 16GB of memory.

Details of baselines

In our evaluation, we conducted a comparison between our system and two baseline methods: mmHRV[24] and V2iFi[25]. These two methods represent the latest approaches for HRV estimation. mmHRV extracts the fundamental frequency components of heartbeats from the signal in the frequency band where heartbeats reside using an optimized algorithm. V2iFi integrates heartbeat information from multiple reflected signals and extracts the fundamental frequency components of heartbeats through signal decomposition. Both methods aim to extract heartbeat information in the low-frequency range through signal decomposition, however, due to the interference of respiratory leakage, they cannot achieve good performance, especially in large populations. The comparative summary of the baselines and our method has been included in Supplementary Note 9.

Evaluation metrics

Evaluation HRV. To better evaluate the capability of the HRV monitoring, we further process the IBIs sequence to RT-IBI. Moreover, we adopt the three most widely used metrics, i.e., RMSSD, SDRR, and pNN50 to evaluate the HRV estimation performance[33].

RT-IBI is utilized to measure the time interval between heartbeats. By taking the difference between the moments when consecutive heartbeats occur, we can obtain the IBIs. Then we further process the IBIs sequence to RT-IBI, a 2-dimensional line chart, where the horizontal axis of each point on the line represents each moment, and the vertical axis represents the IBI at that moment (See the detailed of the generating RT-IBI in Supplementary Note 6 and Fig. 5).

RMSSD is used to measure the successive IBI changes and can be calculated by

$$\text{RMSSD} = \sqrt{\frac{1}{n-1}\sum_{i=2}^{n}(\text{IBI}_{(i)} - \text{IBI}_{(i-1)})^2}, \tag{1}$$

where n denotes the total number of IBIs, $\text{IBI}_{(i)}$ is the ith IBI estimation.

SDRR measures the variation of the IBIs, which can be calculated as

$$\text{SDRR} = \sqrt{\frac{1}{n}\sum_{i=1}^{n}(\text{IBI}_{(i)} - \overline{\text{IBI}})^2}, \tag{2}$$

where $\overline{\text{IBI}}$ is the empirical mean of the IBIs of each measurement.

pNN50 measures the percentage of successive IBI that differ by more than 50 ms, which can be calculated by

$$\text{pNN50} = \frac{\sum_{i=2}^{n}\mathbb{I}(\text{IBI}_{(i)} - \text{IBI}_{(i-1)} > 50\text{ms})}{n}, \tag{3}$$

where $\mathbb{I}$ is the indicator function.

Reporting summary

Further information on research design is available in the Nature Portfolio Reporting Summary linked to this article.

Data availability

The minimum dataset supporting the findings and the released code has been deposited in (https://doi.org/10.24433/CO.9082638.v4). Additional data are available under restricted access due to privacy regulations. Access requests can be directed to the corresponding author, with an expected response time of up to 60 days. Requesters should sign a data use agreement and submit a research proposal specifying the intended use. Access approval is contingent upon an ethical review to ensure compliance with institutional policies and legal requirements. Approved data use will be restricted to non-commercial research purposes. Source data are provided with this paper.

Code availability

The code developed to support the findings of this study is available online at (https://doi.org/10.24433/CO.9082638.v4).

References

1. Economic impacts of cardiovascular diseases. https://www.ncbi.nlm.nih.gov/pmc/articles/PMC9941436/. Accessed February 3, 2024.
2. Roth, G. A. et al. The burden of cardiovascular diseases among us states, 1990-2016. *JAMA Cardiol.* **3**, 375–389 (2018).
3. Cardiovascular diseases. https://www.who.int/health-topics/cardiovascular-diseases#tab=tab_1. Accessed February 3, 2024.
4. Cardiovascular diseases (CVDs). https://www.who.int/news-room/fact-sheets/detail/cardiovascular-diseases-(cvds). Accessed February 3, 2024.
5. Cardiovascular diseases: Avoiding heart attacks and strokes. https://www.who.int/news-room/questions-and-answers/item/cardiovascular-diseases-avoiding-heart-attacks-and-strokes. Accessed February 3, 2024.
6. Calkins, H. et al. Treatment of atrial fibrillation with antiarrhythmic drugs or radiofrequency ablation: two systematic literature reviews and meta-analyses. *Circ.: Arrhythm. Electrophysiol.* **2**, 349–361 (2009).
7. Martin, D. T. et al. Randomized trial of atrial arrhythmia monitoring to guide anticoagulation in patients with implanted defibrillator and cardiac resynchronization devices. *Eur. Heart J.* **36**, 1660–1668 (2015).
8. Page, R. L., Wilkinson, W. E., Clair, W. K., McCarthy, E. A. & Pritchett, E. Asymptomatic arrhythmias in patients with symptomatic paroxysmal atrial fibrillation and paroxysmal supraventricular tachycardia. *Circulation* **89**, 224–227 (1994).
9. Ribeiro, A. H. et al. Automatic diagnosis of the 12-lead ECG using a deep neural network. *Nat. Commun.* **11**, 1760 (2020).
10. DiMarco, J. P. & Philbrick, J. T. Use of ambulatory electrocardiographic (Holter) monitoring. *Ann. Intern. Med.* **113**, 53–68 (1990).
11. Serhani, M. A., T. El Kassabi, H., Ismail, H. & Nujum Navaz, A. Ecg monitoring systems: Review, architecture, processes, and key challenges. *Sensors* **20**, 1796 (2020).
12. Parak, J. et al. Evaluation of the beat-to-beat detection accuracy of pulse on wearable optical heart rate monitor. In *2015 37th Annual International Conference of the IEEE Engineering in Medicine and Biology Society (EMBC)*, 8099–8102 (2015).
13. Kroll, R. R., Boyd, J. G. & Maslove, D. M. Accuracy of a wrist-worn wearable device for monitoring heart rates in hospital inpatients: a prospective observational study. *J. Med. Internet Res.* **18**, e253 (2016).
14. Jeong, H., Kim, H., Kim, R., Lee, U. & Jeong, Y. Smartwatch wearing behavior analysis: a longitudinal study. *Proc. ACM Interact. Mob. Wear. Ubiquitous Technol.* **1**, 1–31 (2017).
15. Charlton, P. H. & Marozas, V. Wearable photoplethysmography devices. In *Photoplethysmography*, 401–439 (Elsevier, 2022).
16. Van Voorhees, E. E. et al. Ambulatory heart rate variability monitoring: Comparisons between the Empatica E4 wristband and Holter electrocardiogram. *Psychosom. Med.* **84**, 210–214 (2022).
17. Castaneda, D., Esparza, A., Ghamari, M., Soltanpur, C. & Nazeran, H. A review on wearable photoplethysmography sensors and their potential future applications in health care. *Int. J. Biosens. Bioelectron.* **4**, 195–202 (2018).
18. Fan, X., Pearl, D., Howard, R., Shangguan, L. & Thormundsson, T. Apg: Audioplethysmography for cardiac monitoring in hearables. In *Proceedings of the 29th Annual International Conference on Mobile Computing and Networking*, 1–15 (2023).
19. Chan, J. et al. An off-the-shelf otoacoustic-emission probe for hearing screening via a smartphone. *Nat. Biomed. Eng.* **6**, 1203–1213 (2022).
20. Zhao, M., Hoti, K., Wang, H., Raghu, A. & Katabi, D. Assessment of medication self-administration using artificial intelligence. *Nat. Med.* **27**, 727–735 (2021).
21. Will, C. et al. Radar-based heart sound detection. *Sci. Rep.* **8**, 11551 (2018).
22. Xia, Z., Shandhi, M. M. H., Inan, O. T. & Zhang, Y. Non-contact sensing of Seismocardiogram signals using microwave Doppler radar. *IEEE Sens. J.* **18**, 5956–5964 (2018).
23. Ha, U., Assana, S. & Adib, F. Contactless seismocardiography via deep learning radars. In *Proceedings of the 26th Annual International Conference on Mobile Computing and Networking*, 1–14 (2020).
24. Wang, F., Zeng, X., Wu, C., Wang, B. & Liu, K. R. MMHRV: Contactless heart rate variability monitoring using millimeter-wave radio. *IEEE Internet Things J.* **8**, 16623–16636 (2021).
25. Zheng, T., Chen, Z., Cai, C., Luo, J. & Zhang, X. V2ifi: In-vehicle vital sign monitoring via compact RF sensing. *Proc. ACM Interact. Mob. Wear. Ubiquitous Technol.* **4**, 1–27 (2020).
26. Zhang, J., Wu, Y., Chen, Y. & Chen, T. Health-radio: Towards contactless myocardial infarction detection using radio signals. *IEEE Trans. Mob. Comput.* **21**, 585–597 (2020).
27. Bigger, J., Fleiss, J. L., Rolnitzky, L. M. & Steinman, R. C. The ability of several short-term measures of RR variability to predict mortality after myocardial infarction. *Circulation* **88**, 927–934 (1993).
28. Huikuri, H. V. et al. Heart rate variability and progression of coronary atherosclerosis. *Arterioscler. Thromb. Vasc. Biol.* **19**, 1979–1985 (1999).
29. Janszky, I. et al. Heart rate variability in long-term risk assessment in middle-aged women with coronary heart disease: The Stockholm female coronary risk study. *J. Intern. Med.* **255**, 13–21 (2004).
30. Nolan, J. et al. Prospective study of heart rate variability and mortality in chronic heart failure: results of the United Kingdom heart failure evaluation and assessment of risk trial (uk-heart). *Circulation* **98**, 1510–1516 (1998).
31. Sharma, P., Zhang, Z., Conroy, T. B., Hui, X. & Kan, E. C. Attention detection by heartbeat and respiratory features from radio-frequency sensor. *Sensors* **22**, 8047 (2022).
32. Zhang, S., Zheng, T., Chen, Z. & Luo, J. Can we obtain fine-grained heartbeat waveform via contact-free rf-sensing? In *IEEE INFOCOM 2022-IEEE conference on computer communications*, 1759–1768 (IEEE, 2022).
33. Shaffer, F. & Ginsberg, J. P. An overview of heart rate variability metrics and norms. *Front. Public Health* **5**, 258 (2017).
34. Bent, B., Goldstein, B. A., Kibbe, W. A. & Dunn, J. P. Investigating sources of inaccuracy in wearable optical heart rate sensors. *NPJ Digit. Med.* **3**, 18 (2020).
35. Zhang, D., Hu, Y. & Chen, Y. Mtrack: Tracking multiperson moving trajectories and vital signs with radio signals. *IEEE Internet Things J.* **8**, 3904–3914 (2020).
36. Yue, S., He, H., Wang, H., Rahul, H. & Katabi, D. Extracting multi-person respiration from entangled RF signals. *Proc. ACM Interact. Mob. Wear. Ubiquitous Technol.* **2**, 1–22 (2018).
37. Xiao, Y., Lin, J., Boric-Lubecke, O. & Lubecke, M. Frequency-tuning technique for remote detection of heartbeat and respiration using low-power double-sideband transmission in the ka-band. *IEEE Trans. Microw. Theory Tech.* **54**, 2023–2032 (2006).
38. Chen, J. et al. Contactless electrocardiogram monitoring with millimeter wave radar. *IEEE Trans. Mob. Comput.* **23**, 270–285 (2022).
39. Ling, Z., Zhou, W., Ren, Y., Wang, J. & Guo, L. Non-contact heart rate monitoring based on millimeter wave radar. *IEEE Access* **10**, 74033–74044 (2022).
40. Liu, J., Li, Y., Li, C., Gu, C. & Mao, J.-F. Accurate measurement of human vital signs with linear FMCW radars under proximity stationary clutters. *IEEE Trans. Biomed. Circuits Syst.* **15**, 1393–1404 (2021).

41. Islam, S. M. M., Motoyama, N., Pacheco, S. & Lubecke, V. M. Non-contact vital signs monitoring for multiple subjects using a millimeter wave FMCW automotive radar. In *2020 IEEE/MTT-S International Microwave Symposium (IMS)*, 783–786 (2020).

42. Rong, Y. & Bliss, D. W. Remote sensing for vital information based on spectral-domain harmonic signatures. *IEEE Trans. Aerosp. Electron. Syst.* **55**, 3454–3465 (2019).

43. Xu, H. et al. Accurate heart rate and respiration rate detection based on a higher-order harmonics peak selection method using radar non-contact sensors. *Sensors* **22**, 83 (2021).

44. Wu, K. J. & Yang, C.-L. Heart rate extraction with vmd algorithm in non-stationary clutter environment based on FMCW radar systems. In *2021 IEEE International Symposium on Radio-Frequency Integration Technology (RFIT)*, 1–3 (IEEE, 2021).

45. Balasooriya, T., Nallabolu, P. & Li, C. Application of variational mode decomposition to FMCW radar interference mitigation. In *Sensing Technology: Proceedings of ICST 2022*, 425–432 (Springer, 2022).

46. Robey, F. C., Fuhrmann, D. R., Kelly, E. J. & Nitzberg, R. A CFAR adaptive matched filter detector. *IEEE Trans. Aerosp. Electron. Syst.* **28**, 208–216 (1992).

47. Mohd Apandi, Z. F., Ikeura, R., Hayakawa, S. & Tsutsumi, S. An analysis of the effects of noisy electrocardiogram signal on heartbeat detection performance. *Bioengineering* **7**, 53 (2020).

48. Dragomiretskiy, K. & Zosso, D. Variational mode decomposition. *IEEE Trans. Signal Process.* **62**, 531–544 (2013).

49. Zhu, L. & Liu, C. Recent progress of chatter prediction, detection and suppression in milling. *Mech. Syst. Signal Process.* **143**, 106840 (2020).

50. Zhou, F., Huang, Z. & Zhang, C. Carbon price forecasting based on CEEMDAN and LSTM. *Appl. Energy* **311**, 118601 (2022).

Acknowledgements

Author contributions

Y.C., B.Z., Q.S., and L.M. conceived and designed the research. B.Z. devised the methodology and conducted the validation experiments. B.Z., Y.L., Y.H., and Y.C. participated in drafting the paper and approved the final version of the manuscript. D.Z. and Z.L. provided support for the method design. J.C., H.W., F.Z., and Y.P. offered valuable assistance with experimental validation. Y.C. supervised the work.

Competing interests

The authors declare no competing interests.

Ethics statement and informed consent

The project was conducted after an ethics review by the Ethics Review Board of The First Affiliated Hospital of the University of Science and Technology of China. When registering, all participants agreed that their data could be used for scientific research and signed an informed consent form. Participants received no compensation for their participation.

Additional information

Supplementary information The online version contains supplementary material available at https://doi.org/10.1038/s41467-024-55061-9.

Correspondence and requests for materials should be addressed to Yan Chen.

Peer review information *Nature Communications* thanks Jianlin Zhou, Zijing Zhang, and the other, anonymous, reviewer(s) for their contribution to the peer review of this work. A peer review file is available.

Reprints and permissions information is available at http://www.nature.com/reprints

Publisher's note Springer Nature remains neutral with regard to jurisdictional claims in published maps and institutional affiliations.